GROUND DATA PROCESSING &
PRODUCTION OF THE LEVEL 1 HIGH RESOLUTION MAPS

VALERI 2003

LAROSE site
(boreal forest)
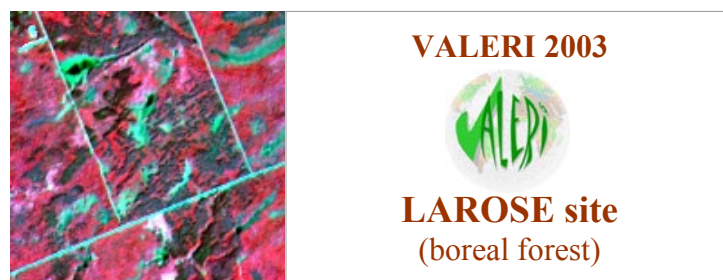
Philippe Rossello, Marie Weiss

November 2005

CONTENTS

1. Introduction

This report describes the production of the high resolution, level 1, biophysical variable maps for the Larose site in 2003 (see campaign report for more details about the site and the ground measurement campaign: annex or http://www.avignon.inra.fr/valeri). Level 1 map corresponds to the map derived from the determination of a transfer function between reflectance values of the SPOT image acquired during (or around) the ground campaign, and biophysical variable measurements (hemispherical images). For each Elementary Sampling Unit (ESU), the hemispherical images were processed using the CAN-EYE software (Version 4.1) developed at INRA-CSE. The derived biophysical variable maps are:

• four Leaf Area Index (LAI) are considered: effective LAI (LAIeff) and true LAI (LAItrue) derived from the description of the gap fraction as a function of the view zenith angle; effective LAI57 (LAI57eff) and true LAI57 (LAI57true) derived from the gap fraction at 57.5°, which is independent on the leaf inclination. Effective LAI and effective LAI57 do not take into account clumping effect. LAItrue and LAI57true are derived using the method proposed by Lang and Yueqin[1] (1986);

• cover fraction (fCover): it is the percentage of soil covered by vegetation. To improve the spatial sampling, fCover was computed over 0 to 10° zenith angle;

• fAPAR: it is the fraction of Absorbed Photosynthetically Active Radiation (PAR=400-700nm). The fAPAR is defined either instantaneously (for a given solar position) or integrated all over the day. Following a study based on radiative transfer model simulations, it has been shown that the root mean square error between instantaneous fAPAR computed every 30 minutes and the daily fAPAR is the lowest for instantaneous fAPAR at 10h00 AM (solar time, RMSE = 0.021). Therefore, the derivation of fAPAR from CAN-EYE corresponds to the instantaneous black sky fAPAR at 10h00 AM.

The land cover is mainly composed of boreal forest (conifers and deciduous trees) and wetland (grass and shrub). The site is quite flat (for more information, see campaign report: http://www.avignon.inra.fr/valeri).

The site coordinates are described in Table 1:

	UTM, 18 North, WGS84 (units = meters)		Geographic Lat/Lon WGS84 (units = degrees)	
	Northing	Easting	Lat.	Lon.
Upper left corner	5026751	481500	45.394033	-75.236353
Lower right corner	5023751	484500	45.367100	-75.197931
Center	5025251	483000	45.380567	-75.217136

Table 1. Description of the site coordinates.

The ground measurements were carried out from 05/08/2003 to 08/08/2003, while the high spatial resolution image (SPOT4, HRVIR1, resolution: 20 m) was acquired on 19/08/2003. The characteristics of the SPOT image are specified in the campaign report.

2. Available data

2.1. SPOT Image

The SPOT image was acquired the 19th August 2003 by HRVIR1 on SPOT4. It was geo-located by SPOTimage (SPOTView basic) who used a previous LANDSAT image geo-located using Ground Control Points (GCP). The projection is UTM 18 North, WGS-84 (please, refer to the campaign report for more details: http://www.avignon.inra.fr/valeri). No atmospheric correction was applied to the image since no atmospheric data were available. However, as the SPOT image is used to compute empirical relationships between reflectance and biophysical variable, we can assume that the effect of the atmosphere is the same over the whole 3 x 3 km site. Therefore, it will be taken into account everywhere in the same way.

Figure 1 shows the relationship between Red and near infrared (NIR) SPOT channels: the soil line is well marked and no saturated points are observed.

---

[1] Lang, A.R.G. and Yueqin, X., 1986. Estimation of leaf area index from transmission of direct sunlight in discontinuous canopies. Agric. For. Meteorol., 37: 229-243.
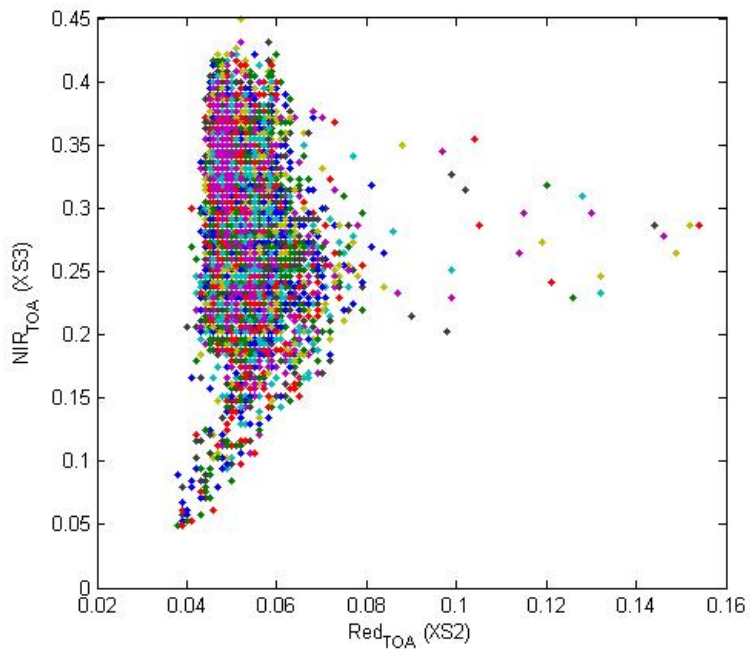
Figure 1. Red/NIR relationship on the SPOT image for Larose, 2003.

2.2. Hemispherical images

The hemispherical images were processed using the CAN-EYE software (Version 4.1) to derive the biophysical variables. A first process was carried out with the Version 1.4. The major improvement between these two versions is that version 4.1 provides estimation of true LAI and clumping effect whereas version 1.4 does not. Figure 2 shows the comparison between the LAIeff results of the hemispherical images processing using two different CAN-EYE versions. The relationship is consistent, even if differences are visible. The "user effect" is probably a determinant factor.
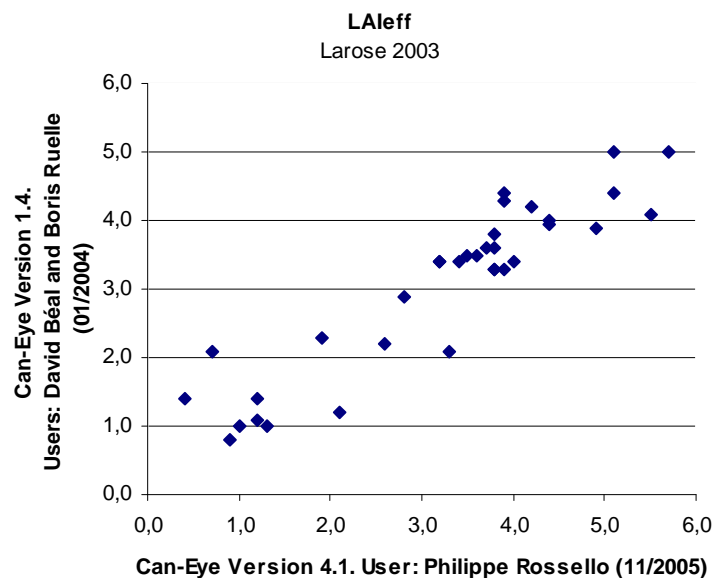

Figure 2. Comparison of CAN-EYE processing results from two versions used by different users (points in blue correspond to 34 ESUs).

Figure 3 and Figure 4 show the distribution of the several variables over the sampled ESUs. As there was understorey on 33 ESUs, hemispherical images were acquired from above the understorey and from below the canopy (trees). The two sets of acquisition were processed separately to derived LAI (effective and true), LAI57 (effective and true), fCover, and fAPAR. The ESU biophysical variable was then computed as:
• LAIeff, LAI57eff, LAItrue, LAI57true: LAI(above) + LAI(below).

• fCover: 1-(1-fCover(above))*(1-fCover(below)). This assumes that independency of the gaps inside the understorey and the gaps inside the trees which is not true at all the scales but it is the only way to get the total fCover. However, for the local scales considered, this might be true as a first order approximation.
• fAPAR: [1-(1-fAPAR(below))*(1-fAPAR(above))], since 1-fAPAR can be considered equivalent to a gap fraction. Here again, the same independency between the two layers has to be assumed.

Note that LAI (effective and true) derived from directional gap fraction and LAI derived from gap fraction at 57.5° (effective and true) are consistent (Figure 3 and Figure 4). Effective LAI (LAIeff, LAI57eff) varies from 0.9 to 5.7, while true LAI (LAItrue, LAI57true) varies from 1.59 to 10.37. This range shows a quite homogeneous site in terms of LAI. For values, LAIeff and LAI57eff are lower than LAItrue and LAI57true. This is due to the clumping observed for several ESUs. The relationship between fAPAR and LAI is in agreement with what is expected (Beer-Lambert law) while the fCover-LAI relationship is more noisy.

To build the relationships between biophysical variables and SPOT data, the reflectance of a given forest ESU was considered as the average reflectance over the central pixel + the 8 surrounding pixels. This takes into account the fact that the height of the trees are about 20 m and consequently the fish-eye observes an area of $\pi \, x \, [20 \, x \, \tan(60°)]^2 \cong 3800 \, m^2$, *i.e.* close to the area of 9 SPOT pixels (=3600m²) when using a maximum view zenith angle of 60°.
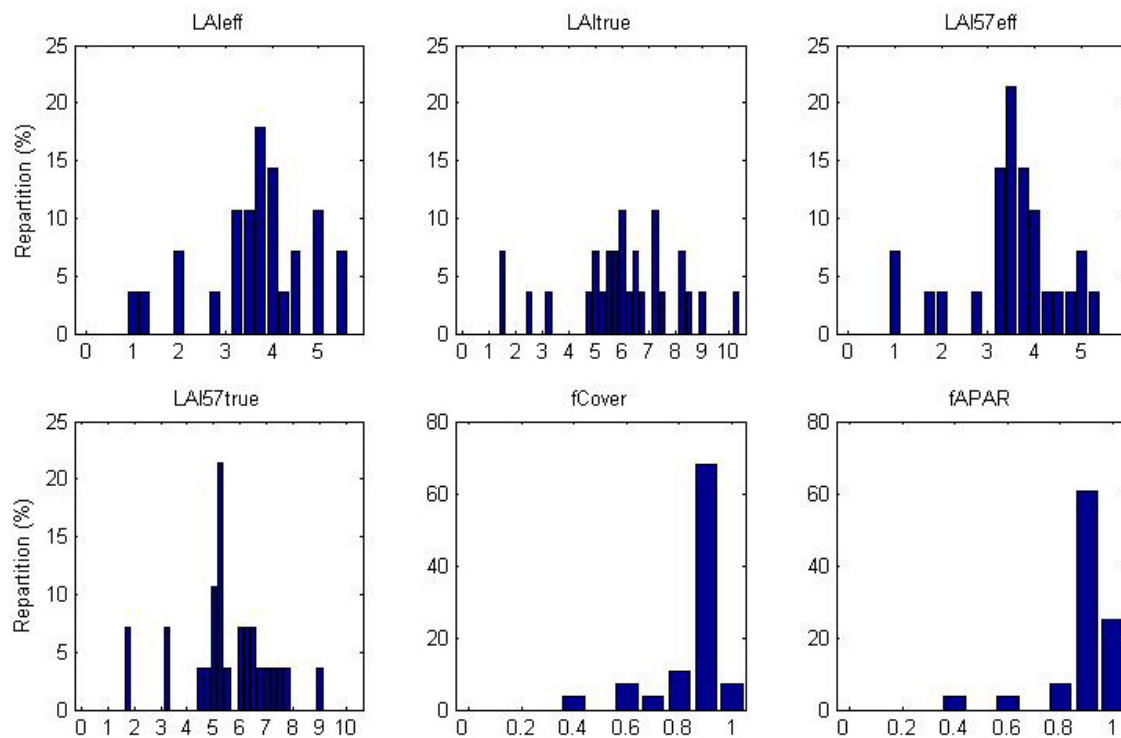

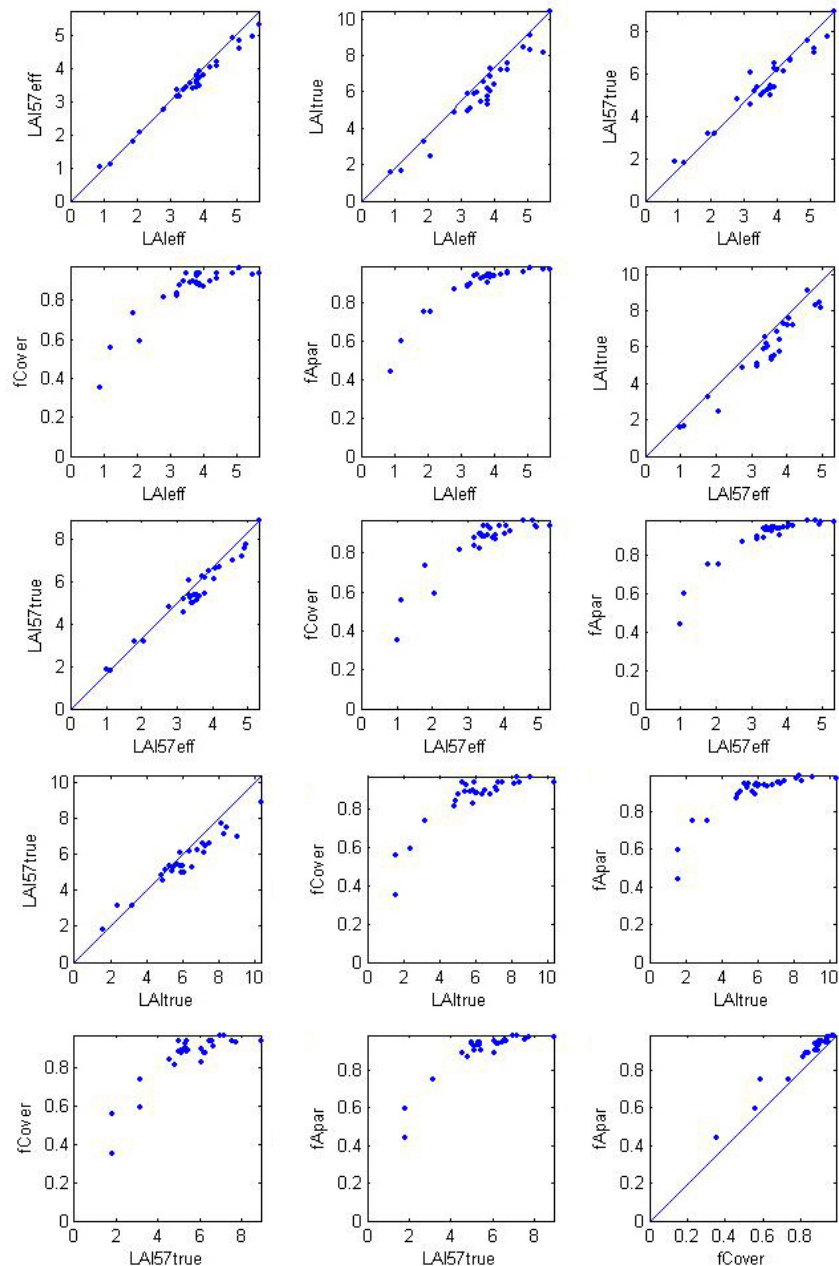**Figure 3. Distribution of the measured biophysical variables over the ESUs.**

Figure 4. Relationships between the different biophysical variables

2.3. Sampling strategy

2.3.1. Principles

The sampling strategy is defined in the campaign report: http://www.avignon.inra.fr/valeri. The sampling of each ESU is based on sixteen elementary photographs.

Figure 5 shows that the 34 ESUs are evenly distributed over the site (3 x 3 km). The processing of the ground data has shown that:

• ESUs E3, E19, E30, E31 (in black on Figure 5) were located very close to the road and sometimes hemispherical images were acquired over the road which does not really make sense for the processing. E14 and E24 (in black on Figure 5) were located on a small plot with a strong heterogeneity on the borders with the presence of surface water. These six ESUs were eliminated;

• considering that SPOT geo-location and GPS measurements are associated to errors, we found that processed LAI for ESUs E9, E13, E18 and E20 did not correspond to the SPOT pixel in terms of reflectance as compared to the knowledge of the land use: according with the people who acquired the data, they have been shifted by 1 pixel.

Finally 28 ESUs have been kept for the computation of the transfer function.
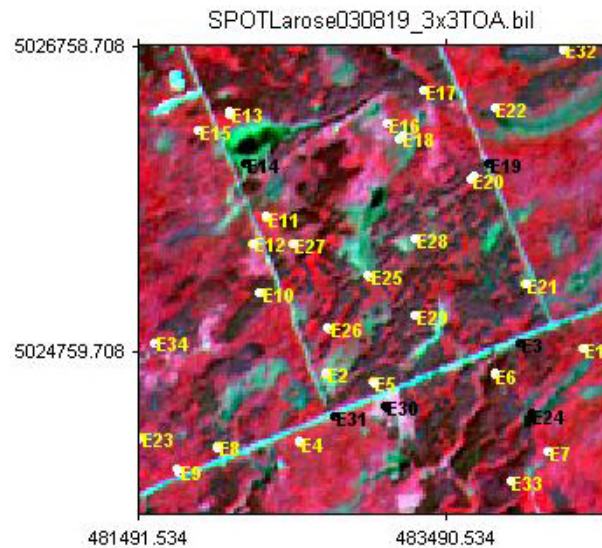

Figure 5. Distribution of the ESUs around the Larose site. ESUs in black (E3, E14, E19, E24, E30, E31) were eliminated for the computation of the transfer function.

The land cover map of the Larose site is available in the report on measurement campaign (annex or http://www.avignon.inra.fr/valeri).

2.3.2. Evaluation based on NDVI values

The sampling strategy is evaluated using the SPOT image by comparing the NDVI distribution over the site with the NDVI distribution over the ESUs (Figure 6). As the number of pixels is drastically different for the ESU and whole site (WS=22500 in case of a 3 x 3 km SPOT image), it is not statistically consistent to directly compare the two NDVI histograms. Therefore, the proposed technique consists in comparing the NDVI cumulative frequency of the two distributions by a Monte-Carlo procedure which aims at comparing the actual frequency to randomly shifted sampling patterns. It consists in:

1. computing the cumulative frequency of the N pixel NDVI that correspond to the exact ESU locations;
2. then, applying a unique random translation to the sampling design (modulo the size of the image);
3. computing the cumulative frequency of NDVI on the randomly shifted sampling design;
4. repeating steps 2 and 3, 199 times with 199 different random translation vectors.

This provides a total population of $N = 199 + 1(\text{actual})$ cumulative frequency on which a statistical test at acceptance probability $1 - \alpha = 95\%$ is applied: for a given NDVI level, if the actual ESU density function is between two limits defined by the $N\alpha / 2 = 5$ highest and lowest values of the 200 cumulative frequencies, the hypothesis assuming that WS and ESU NDVI distributions are equivalent is accepted, otherwise it is rejected.
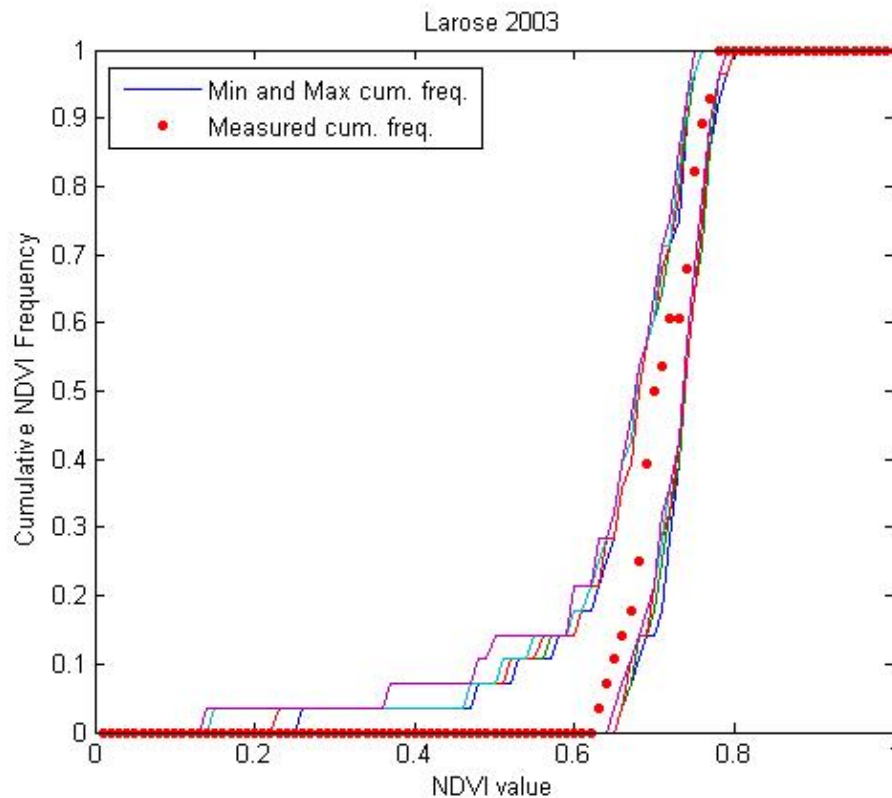
Figure 6. Comparison of the ESU NDVI distribution and the NDVI distribution over the whole image.

Figure 6 shows that the NDVI distribution of the 28 ESUs is quite good over the whole site (comprised between the 5 highest and lowest cumulative frequencies) even if the cumulative frequency curve is close to the boundaries for high NDVI values. Note that NDVIs lower than 0.62 have not been sampled either although they are present in the image (bare soil for example). The site is quite homogeneous in terms of NDVI since the highest and lowest distributions are close.

2.3.3.   Evaluation based on classification

A non supervised classification based on the k_means method (Matlab statistics toolbox) was applied to the reflectance of the SPOT image to distinguish if different behaviours on the image for the biophysical variable-reflectance relationship exist.

A number of 5 classes was chosen (Figure 7). The distribution of the classes on the image and on the ESUs is rather similar. Classes 1, 3 and 4 are under-represented while classes 2 and 5 appear to be over-sampled.
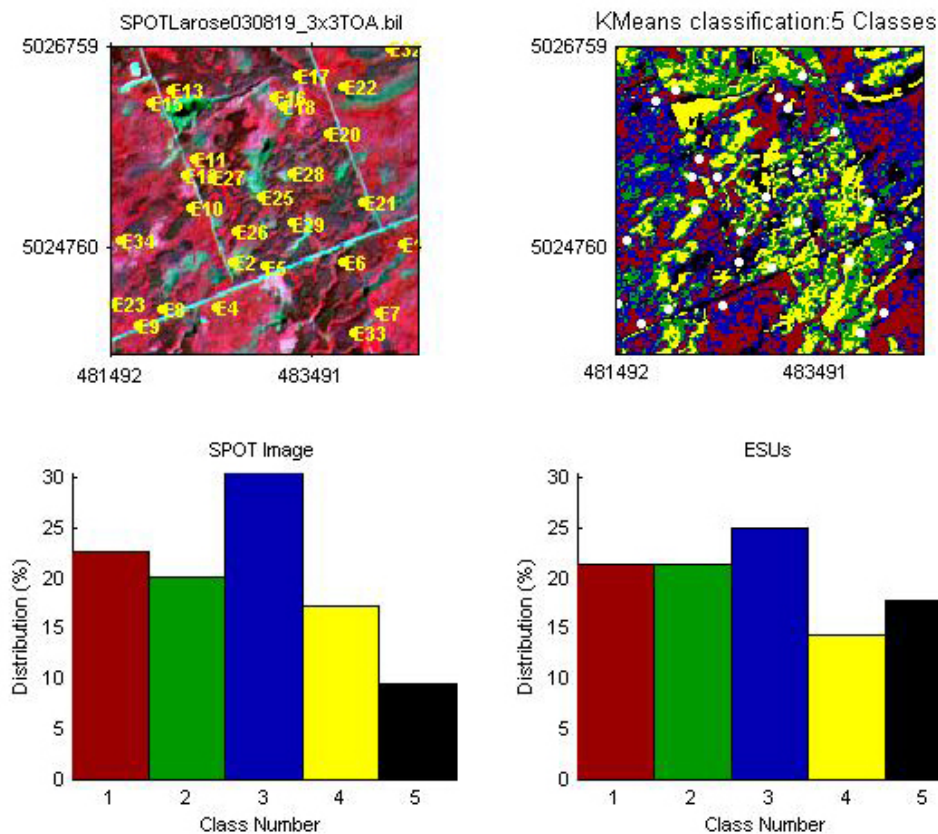
Figure 7. Classification of the SPOT image. Comparison of the class distribution between the SPOT image and sampled ESUs.

Figure 8 shows the different relationships observed between the biophysical variables and the corresponding NDVI on the ESUs, as a function of the SPOT classes determined from non supervised classification.
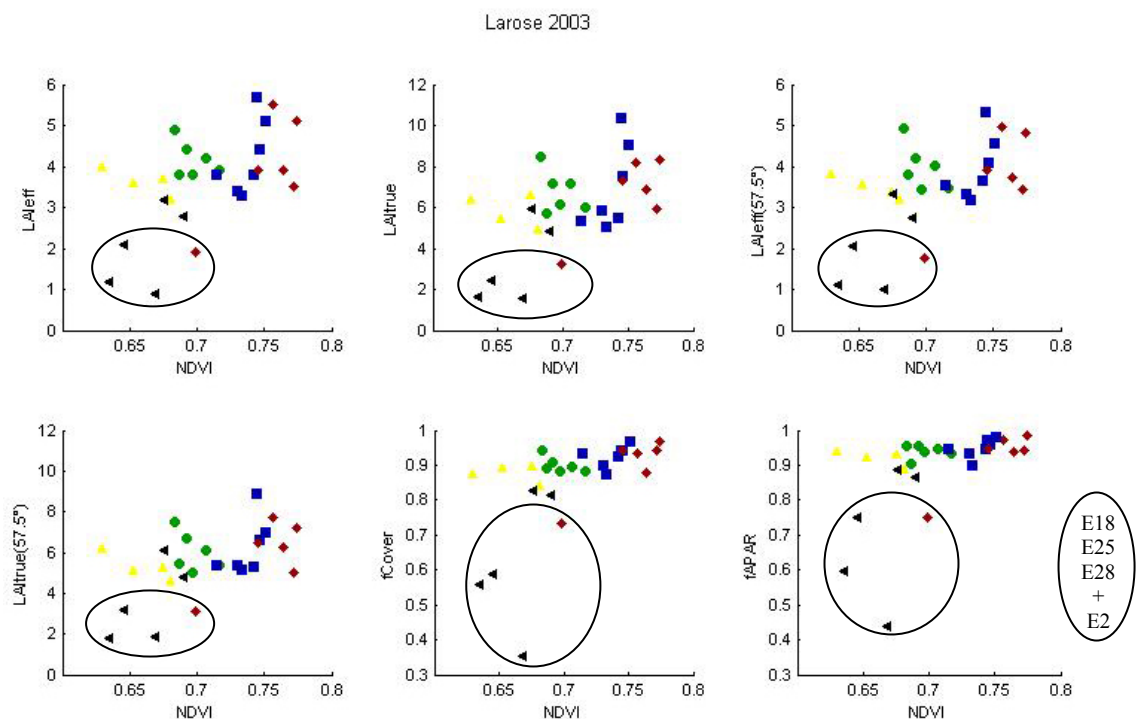

Figure 8. NDVI-Biophysical Variable relationships as a function of SPOT classes

Even if no different behaviour between the classes can be observed, three ESUs (E18, E25, E28 in black class) differ from the others: the biophysical variable values are generally low while NDVIs are high. These

ESUs are characterized by a very wet soil with the presence of surface water. Note that ESU2 (red class) has also a specific behaviour. It is located on a small plot close to the road and wetlands with young trees, a low understorey, grass and an irregular density of the trees. However, a single transfer function per variable will be generated.

2.3.4. Using convex hulls

A test based on the convex hulls was also carried out to characterize the representativeness of ESUs. Whereas the evaluation based on NDVI values uses two bands (red and NIR), this test uses the four bands of the SPOT image. A flag image, is computing over the reflectances (Figure 9). The result on convex-hulls can be interpreted as:

• pixels inside the 'strict convex-hull': a convex-hull is computed using all the SPOT reflectance corresponding to the ESUs belonging to the class. These pixels are well represented by the ground sampling and therefore, when applying a transfer function the degree of confidence in the results will be quite high, since the transfer function will be used as an interpolator;

• pixels inside the 'large convex-hull': a convex-hull is computed using all the reflectance combination (±5% in relative value) corresponding to the ESUs. For these pixels, the degree of confidence in the obtained results will be quite good, since the transfer function is used as an extrapolator (but not far from interpolator);

• pixels outside the two convex-hulls: this means that for these pixels, the transfer function will behave as an extrapolator which makes the results less reliable. However, having a priori information on the site may help to evaluate the extrapolation capacities of the transfer function.
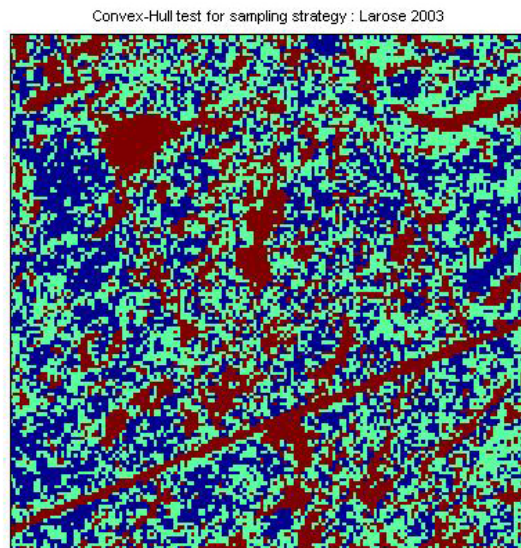

Figure 9. Evaluation of the sampling based on the convex hulls. The map is shown at the bottom: blue and light blue correspond to the pixels belonging to the 'strict' and 'large' convex hulls and red to the pixels for which the transfer function is extrapolating.

This map shows that the representativeness of the ESUs is quite good, even if pixels are outside the two convex-hulls. They correspond to bare soil, road and wetlands.

3. Determination of the transfer function for the 6 biophysical variables: LAIeff, LAI57eff, LAItrue, LAI57true, fCover, fAPAR

3.1. The transfer function considered

For each class determined in §2.3, the following transfer function was tested:

• REG: if the number of ESUs is sufficient, multiple robust regression between ESUs reflectance (or Simple Ratio) and the considered biophysical variable can be applied: we used the 'robustfit' function from the Matlab statistics toolbox. It uses an iteratively re-weighted least squares algorithm, with the weights at each iteration computed by applying the bisquare function to the residuals from the previous iteration. This algorithm provides lower weight to ESUs that do not fit well. The results are less sensitive to outliers in the

data as compared with ordinary least squares regression. At the end of the processing, three errors are computed: classical root mean square error (RMSE), weighted RMSE (using the weights attributed to each ESU) and cross-validation RMSE (leave-one-out method).

The regression is tested using either the reflectance or the logarithm of the reflectance for any band combination as well as the simple ratio or NDVI. As the method has poor extrapolation capacities, a flag image, based on the convex hulls is computing over reflectances.

3.2. Results

3.2.1. Choice of the method

For the 5 classes, a unique transfer function was computed. Figure 10 shows the results obtained for all the possible band combinations using either the reflectance or the logarithm of the reflectance: for LAIeff, LAItrue, LAI57eff, LAI57true, fCover and fAPAR, the results using the reflectance are the best. Depending on the biophysical variable, the choice of the band combinations proves to be difficult because the results are close. Note that the Red*NIR (+ or RN) combination is added to all the band combinations (except for NDVI and SR). Please read the following document: "A method to improve the relation between the biophysical variables" (http://www.avignon.inra.fr/valeri/table_methods/new_linear.pdf).
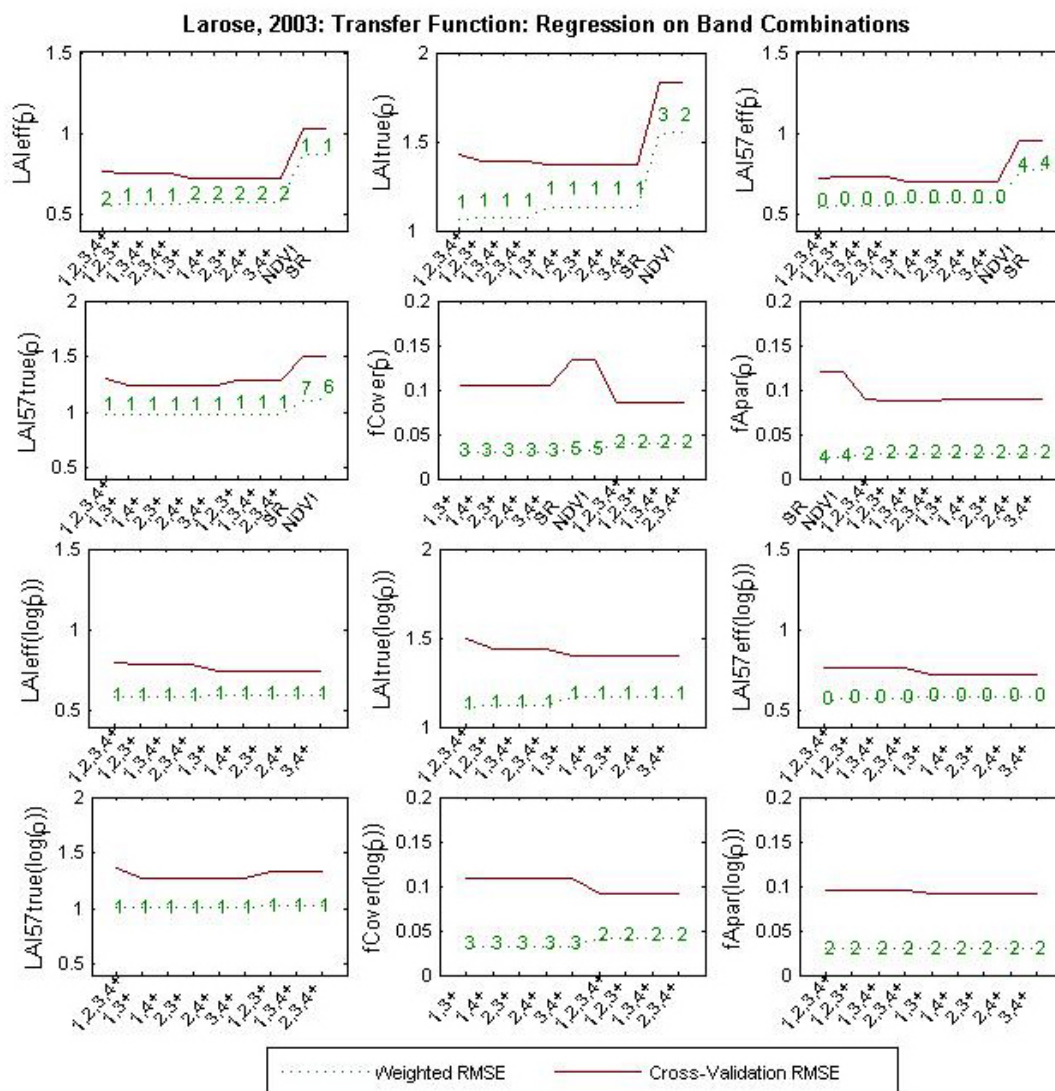

Figure 10. Transfer function: test of multiple regression applied on different band combinations. Band combinations are given in abscissa. The estimated biophysical variable is given in ordinate. Top graphs correspond to regression made on reflectance (ρ): the weighted root mean square error (RMSE) is presented in green along with the cross-validation RMSE in red. The numbers indicate the number of data used for the robust regression with a weight lower than 0.7 that could be considered as outliers. Bottom graphs correspond to regression made on the logarithm of the reflectance.

3.2.2. Choice of the band combination

For the LAIeff, the XS1, XS2, XS3, XS4, RN (Figure 11 and Figure 12) combination on reflectance was selected since it provides a good compromise between the cross-validation RMSE, the number of weights lower than 0.7 (two) and the weighted root mean square error (the lowest value).

Figure 11. Effective Leaf Area Index: results for regression on reflectance using different band combinations. R is the root mean square error computed between LAIeff and estimated LAIeff. WR is the weighted root mean square error and CR is the cross validation root mean square error.

Figure 12. Weights associated to each ESU for the determination of LAIeff transfer function.

For the LAItrue, the XS2, XS3, XS4, RN (Figure 13 and Figure 14) combination on reflectance was selected since it provides a good compromise between the cross-validation RMSE (among the lowest values), the number of weights lower than 0.7 (one) and the weighted root mean square error (among the lowest values). The following band combinations provide the same results: [XS1,XS2,XS3,RN]; [XS1,XS3,XS4,RN].
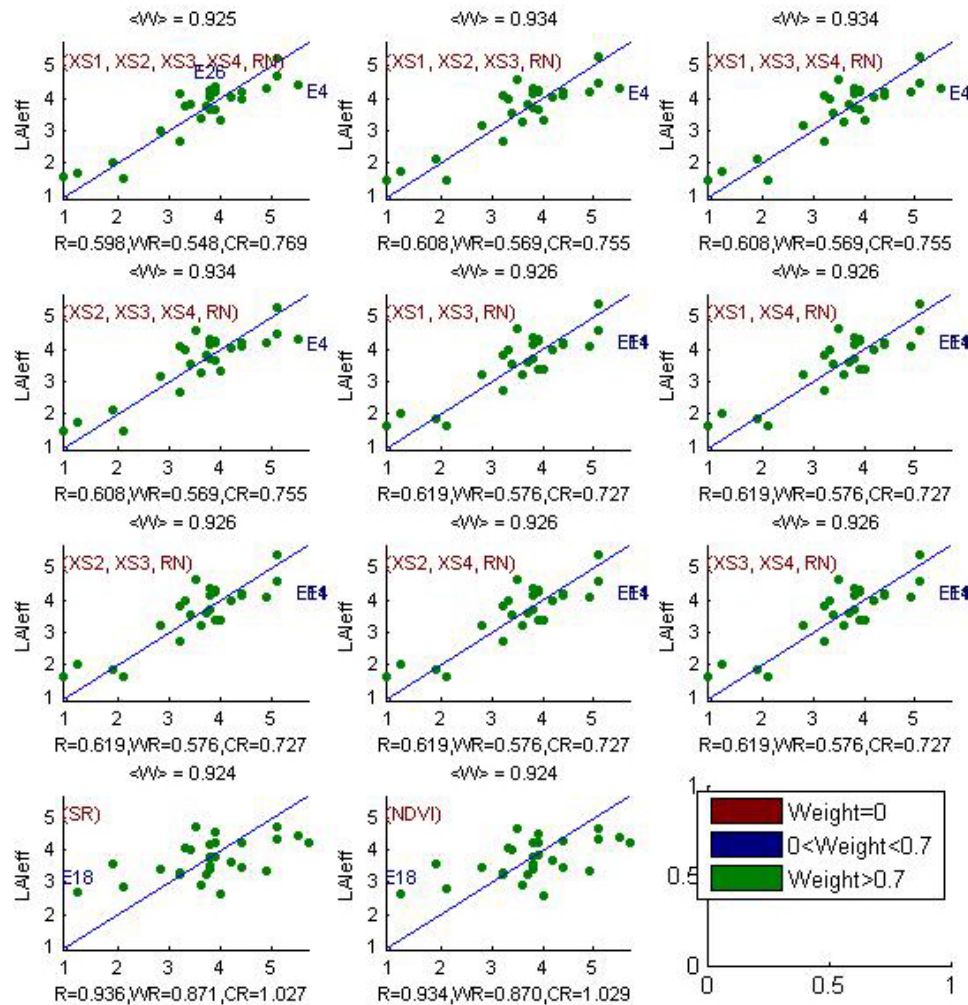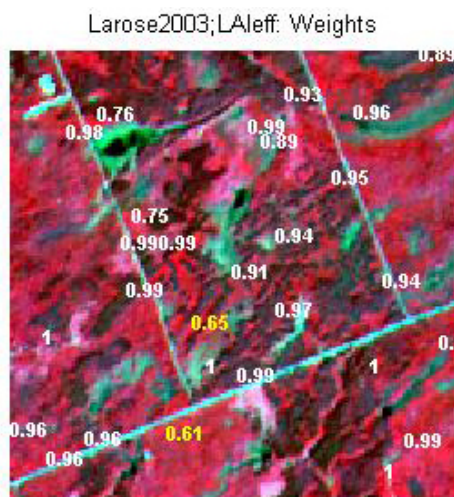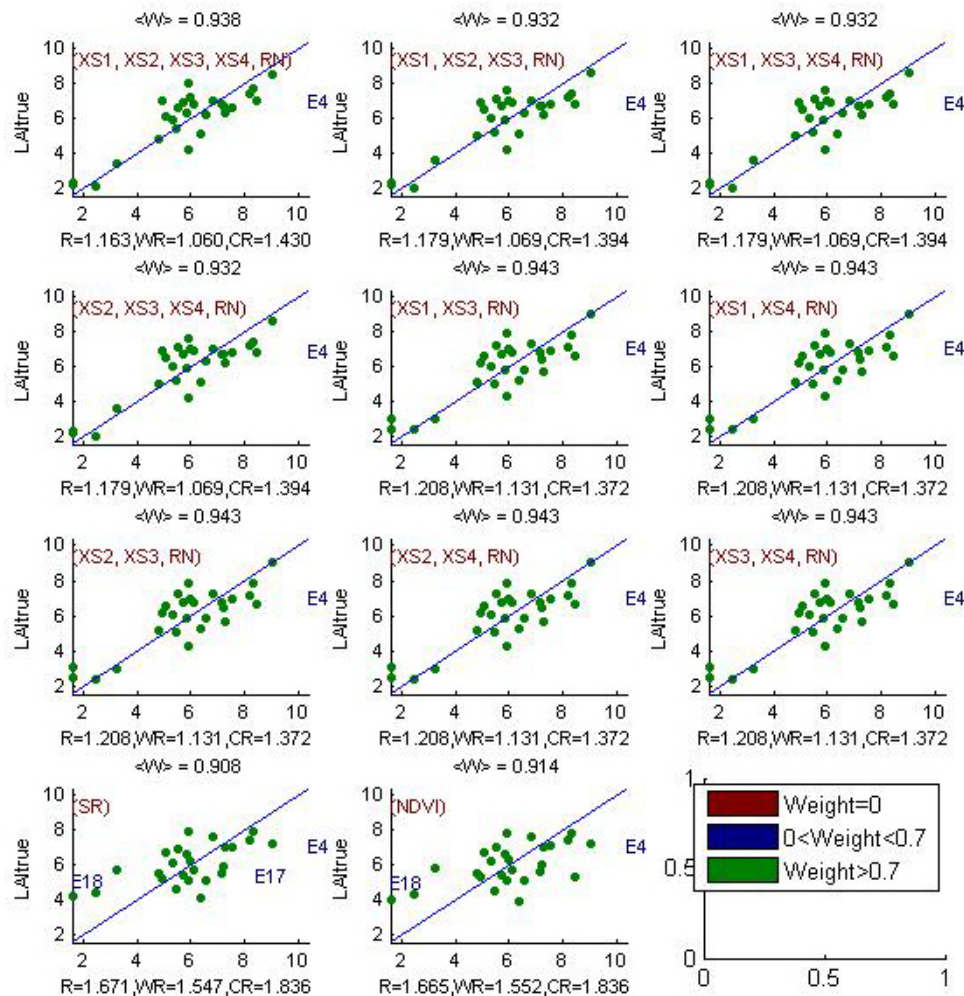

Figure 13. True Leaf Area Index: results for regression on reflectance using different band combinations. R is the root mean square error computed between LAItrue and estimated LAItrue. WR is the weighted root mean square error and CR is the cross validation root mean square error.

Figure 14. Weights associated to each ESU for the determination of LAItrue transfer function.

For the LAI57eff, the XS1, XS2, XS3, XS4, RN (Figure 15 and Figure 16) combination on reflectance was selected since it provides a good compromise between the cross-validation RMSE (among the lowest values), the number of weights lower than 0.7 (zero) and the weighted root mean square error (the lowest value).

Figure 15. Effective LAI at 57.5°: results for regression on reflectance using different band combinations. R is the root mean square error computed between LAI57eff and estimated LAI57eff. WR is the weighted root mean square error and CR is the cross validation root mean square error.
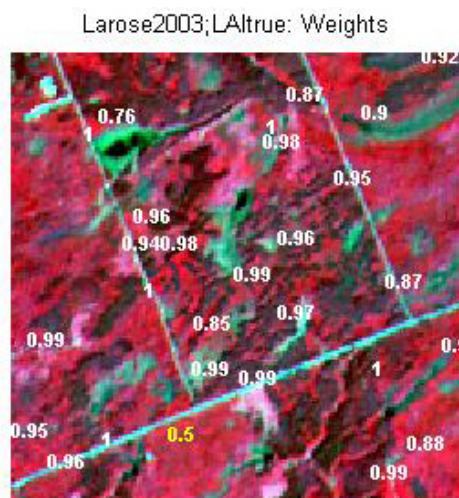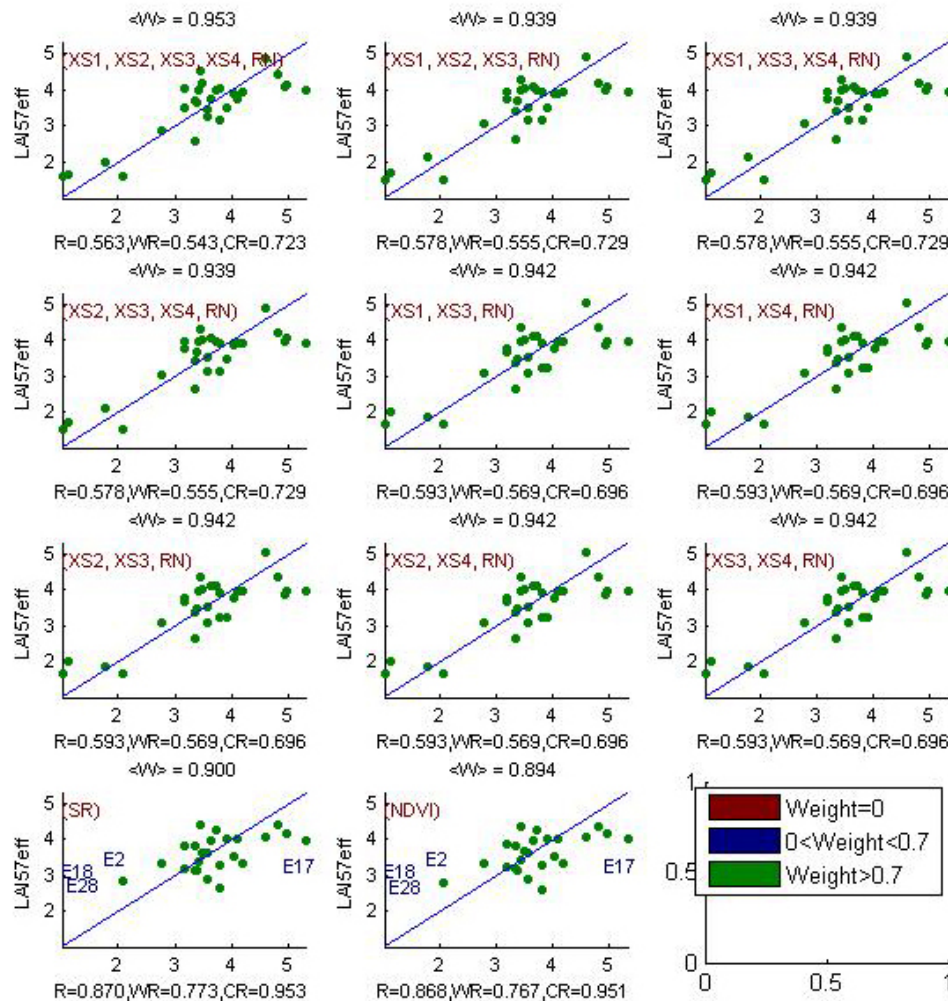

Figure 16. Weights associated to each ESU for the determination of LAI57eff transfer function.

For the LAI57true, the XS3, XS4, RN (Figure 17 and Figure 18) combination on reflectance was selected since it provides a good compromise between the cross-validation RMSE (the lowest value), the number of weights lower than 0.7 (one) and the weighted root mean square error (among the lowest values). The following band combinations provide the same results: [XS1,XS3,RN]; [XS1,XS4,RN] ; [XS2,XS3,RN] ; [XS2,XS4,RN].

Figure 17. True Leaf Area Index at 57.5°: results for regression on reflectance using different band combinations. R is the root mean square error computed between LAI57true and estimated LAI57true. WR is the weighted root mean square error and CR is the cross validation root mean square error.
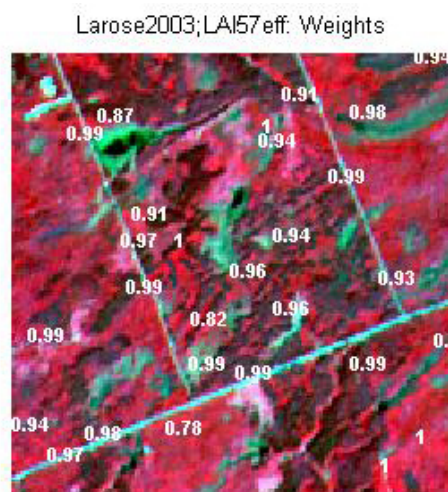

Figure 18. Weights associated to each ESU for the determination of LAI57true transfer function.

For the fCover, the XS1, XS2, XS3, XS4, RN (Figure 19 and Figure 20) combination on reflectance was selected since it provides a good compromise between the cross-validation RMSE (among the lowest values), the number of weights lower than 0.7 (two) and the weighted root mean square error (among the lowest values).

Figure 19. fCover: results for regression on reflectance using different band combinations. R is the root mean square error computed between fCover and estimated fCover. WR is the weighted root mean square error and CR is the cross validation root mean square error.

Figure 20. Weights associated to each ESU for the determination of fCover transfer function.

For the fAPAR, the XS1, XS2, XS3, XS4, RN (Figure 21 and Figure 22) combination on reflectance was selected since it provides a good compromise between the cross-validation RMSE (the lowest value), the number of weights lower than 0.7 (two) and the weighted root mean square error (among the lowest values).

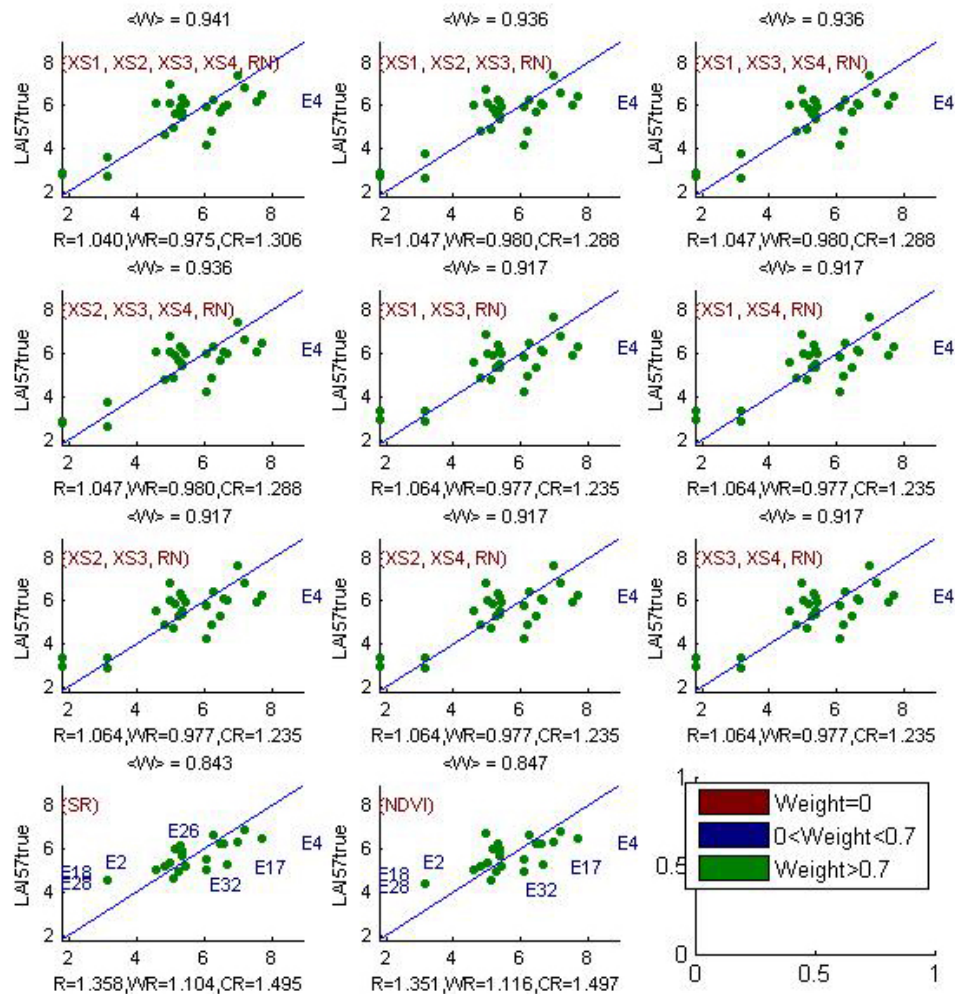**Figure 21. fAPAR: results for regression on reflectance using different band combinations. R is the root mean square error computed between fAPAR and estimated fAPAR. WR is the weighted root mean square error and CR is the cross validation root mean square error.**

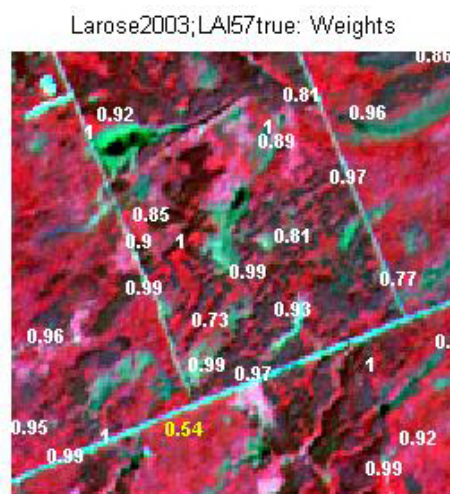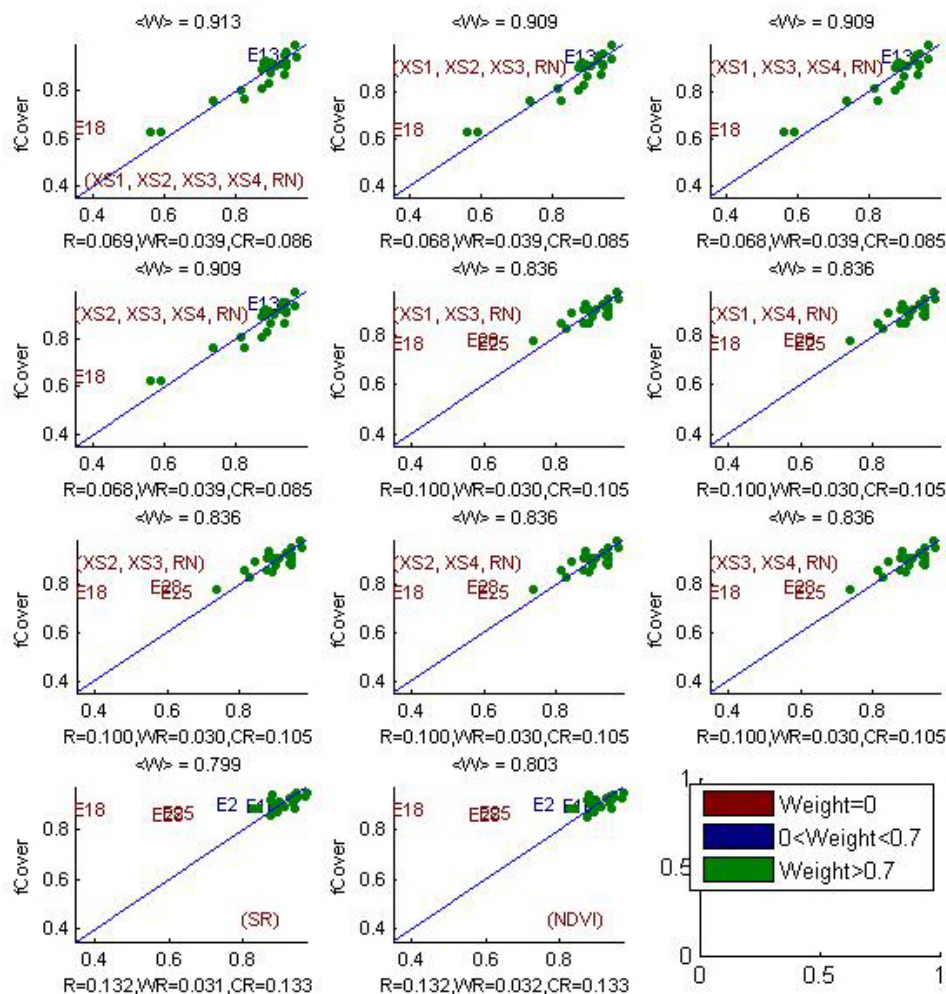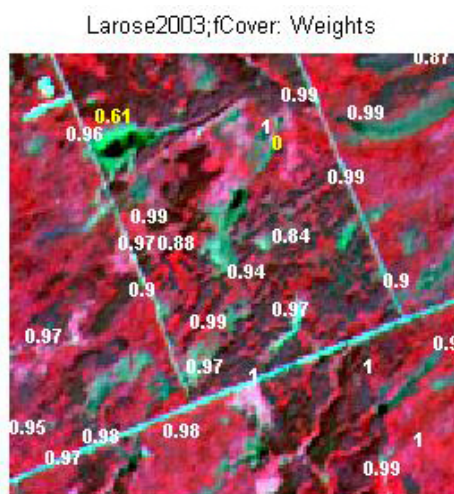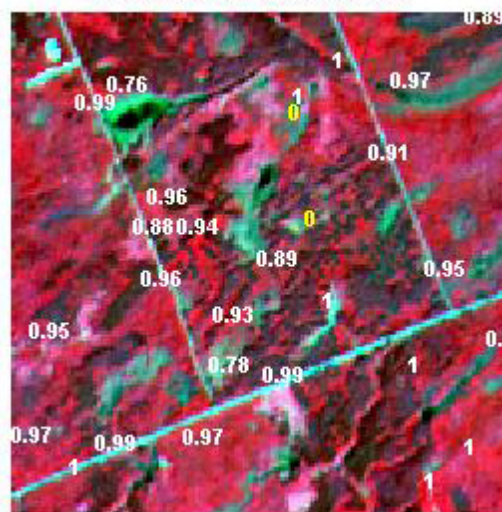**Figure 22. Weights associated to each ESU for the determination of fAPAR transfer function.**

Following, the results of the transfer function (Table 2):

Variable	Band Combination	RMSE	Weighted RMSE	Cross-valid RMSE
LAIeff	12.548 + 187.95(XS1) - 486.95(XS2) - 16.109(XS3) - 11.199(XS4) + 513.68(RN)	0.598	0.548	0.769
LAItrue	58.009 + 309.05(XS2) - 1575.3(XS3) - 142.08(XS4) + 3062.5(RN)	1.179	1.069	1.394
LAI57eff	11.811 + 155.81(XS1) - 423.55(XS2) - 14.431(XS3) - 12.508(XS4) + 482.1(RN)	0.563	0.543	0.723
LAI57true	10.899 + 250(XS3) - 533.14(XS4) + 152.34(RN)	1.064	0.977	1.235
fCover	5.3858 + 14.691(XS1) - 117.07(XS2) - 13.054(XS3) - 0.36682(XS4) + 279.28(RN)	0.069	0.039	0.086
fAPAR	1.4691 + 9.8994(XS1) - 27.678(XS2) - 0.56499(XS3) - 0.47094(XS4) + 21.076(RN)	0.080	0.028	0.088

RN = Red*NIR

Table 2. Transfer function applied to the whole site for the different biophysical variables, and corresponding errors

3.3. Applying the transfer function to the Larose SPOT image extraction

Figure 23 presents the biophysical variable maps obtained with the transfer function described in Table 2. The maps obtained for the six variables are consistent, showing similar patterns: low LAIeff values where low fCover or fAPAR are observed and conversely… The difference between effective LAI and true LAI is significant (see the average values in Figure 23). This was expected when looking the LAIeff/LAItrue relationship, showing that for high LAI the difference between the two can be significant.

Note that a few LAItrue values are very high (up to 14). The pixels are surrounded or very close to surface water where the extrapolation is large (Figure 23). However, their weight is minimal on the scale to the Larose site since they are very located. The LAItrue mean (5.9) is not called into question.
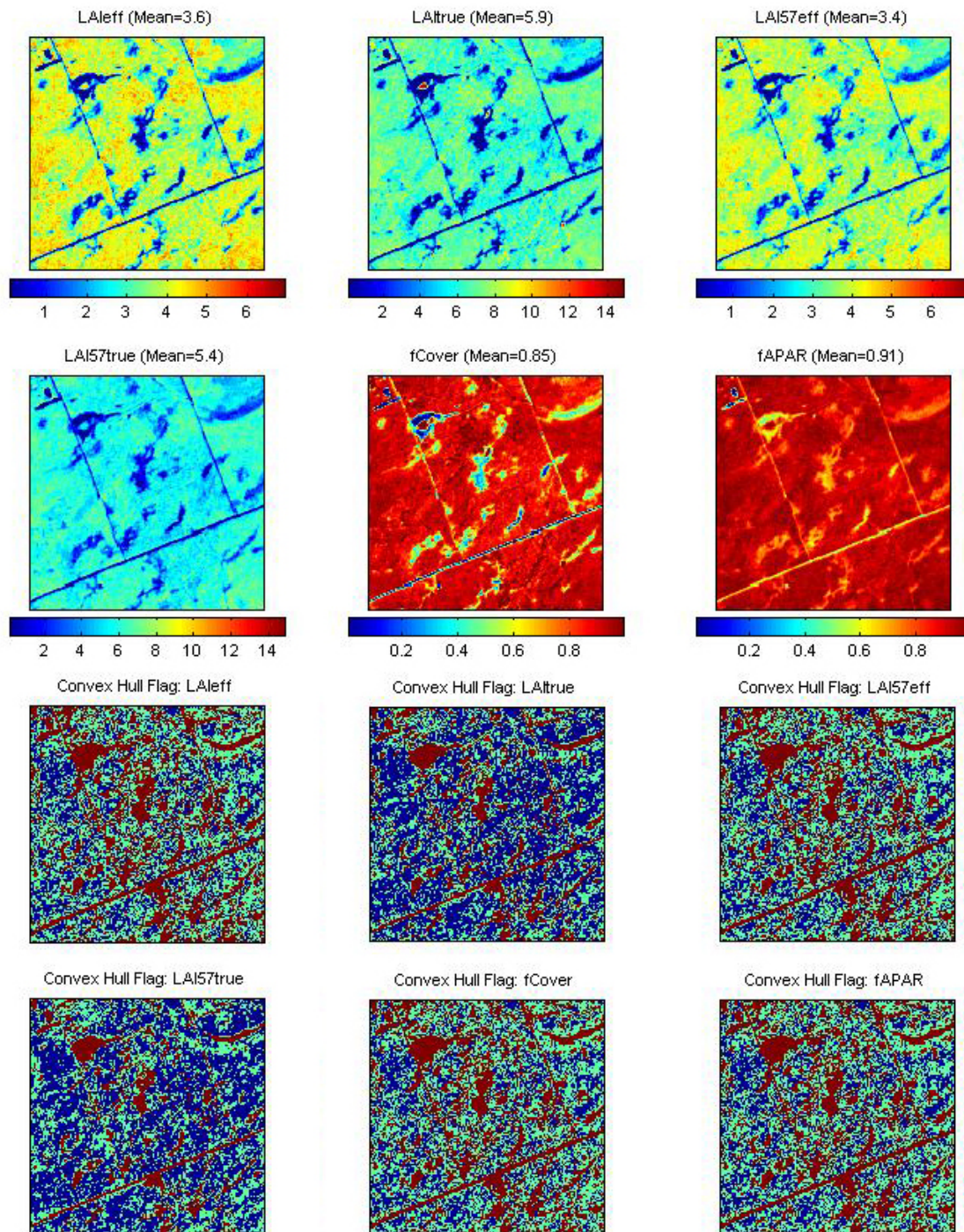
Figure 23. High resolution biophysical variable maps applied on the Larose site (top). Associated Flags are shown at the bottom: blue and light blue corresponds to the pixels belonging to the 'strict' and 'large' convex hulls and red to the pixels for which the transfer function is extrapolating.

The flag maps are different between the biophysical variables since the number and the bands used for the regression are different. The results are comparable between LAIeff, LAI57eff, fCover and fAPAR and between LAItrue and LAI57true. Note that few pixels are outside the strict convex hull for LAItrue and LAI57true. This is due to the choice of the combinations. In theory, the more the number of bands increases, the larger the extrapolation is. The pixels outside the two convex hulls correspond mainly to bare soil, road and wetlands.

4. Conclusion

The transfer functions are obtained by using 28 ESUs. The representativeness of the land cover of the different ESUs is good, even if the bare soil, the wetlands and the road would be worth a best sampling. The results of the robust regression are also good and the maps obtained for the biophysical variables are consistent. The flag associated to each map show that the extrapolation of the transfer function is mainly bounded to bare soil, road and wetlands. Note that the choice of the band combinations (§3.3) is decisive. For all the variables, the regression coefficients are computed by relating the variable itself to reflectance.

The biophysical variable maps are available in UTM, 18 North, projection coordinates (Datum: WGS-84) at 20m resolution.

5. Acknowledgements

ANNEX

Ground measurement acquisition report for the VALERI site
Larose

Sampled from 05/08/2003 to 08/08/2003

David Béal
Organization: INRA
Email: beal@avignon.inra.fr

Date of report 03/09/2003

People participating to the field experiment:

Fistname & Name	0rganization
Richard Fernandès	CCRS, Ontario, Canada
David Béal	INRA CSE, Avignon, France
Leblanc Sylvain	CCRS, Québec, Canada
Jujuan Li	CCRS, Ontario, Canada

Site coordinates

	Lat-Long WGS84 (Decimal Degree)		UTM / WGS84 Zone North 18	
	Lat.	Long.	Easting	Northing
Upper left corner	45.394033	-75.236353	481500	5026751
Lower right corner	45.3671	-75.197931	484500	5023751
Centre	45.380567	-75.217136	483000	5025251

Ground control points

GPSLarose2003.xls contains different GCP's taken on the site (UTM WGS84 North 18): the first two points are T crossing roads, with one common road.

% GCP1	484034	5025375
% GCP2	483300	5024999

GPS system used: Garmin12CX device and Garmin e-Trex devices.
Typical uncertainty of GPS position: 6-7 m.

Description of the site and land cover

Category according to IGBP classification
Forest.

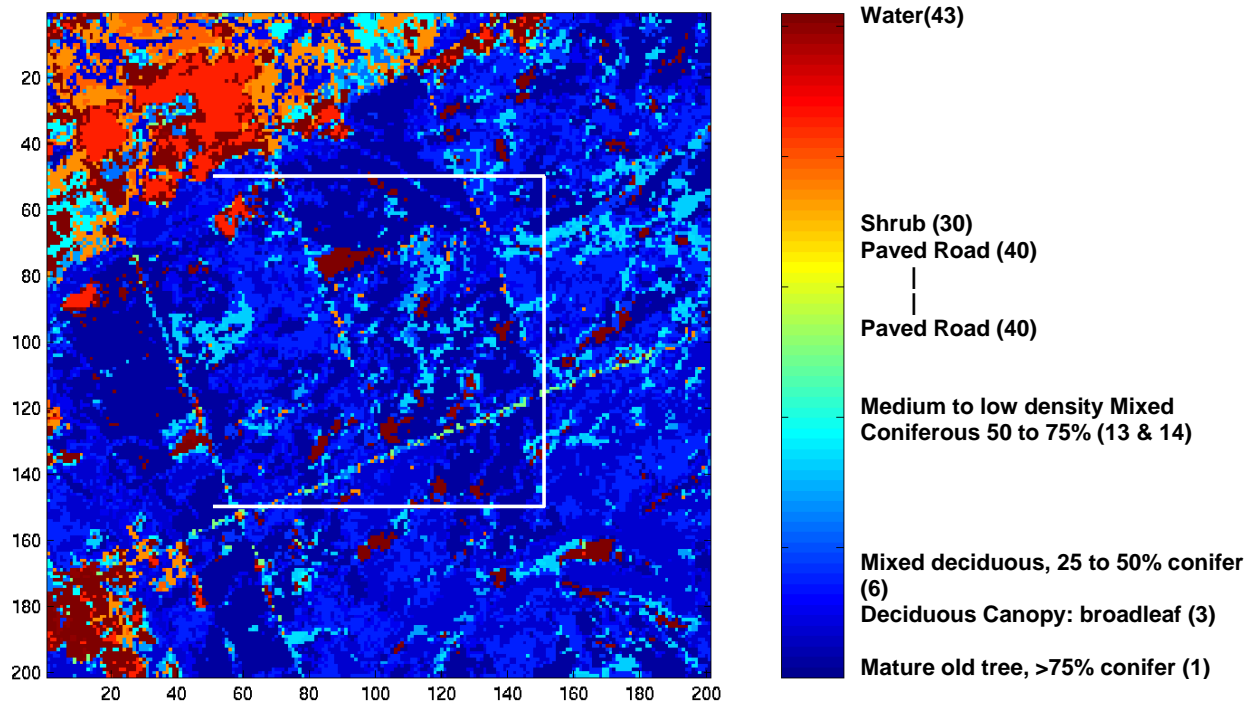## Comments on the land cover
Boreal forest (conifer and deciduous trees) and wetland (grass and shrub).

Topography
The site is generally quite flat.

Land cover map
Numbers in the legend refer to the SILC Land Cover Map for Landsat-7 ETM+ classification. Explanations about that are in the file TMclass_SILC_metadataETM_1629 provided by the CCRS (warning: white square is not exactly VALERI Larose one).

Legend:
- Water(43)
- Shrub (30)
- Paved Road (40)
- |
- |
- Paved Road (40)
- Medium to low density Mixed Coniferous 50 to 75% (13 & 14)
- Mixed deciduous, 25 to 50% conifer (6)
- Deciduous Canopy: broadleaf (3)
- Mature old tree, >75% conifer (1)

Spatial Sampling scheme
Sensors used for sampling the ESUs

	Method	Comments
☒	Hemispherical photographs	
☐	LAI2000	
☐	TRAC	
☐	Ceptometer	
☐	Direct measurements	
☐	Other	

Sampling strategy for the ESU

a	b	c	d
☐	☐	☐	☒ (specify)
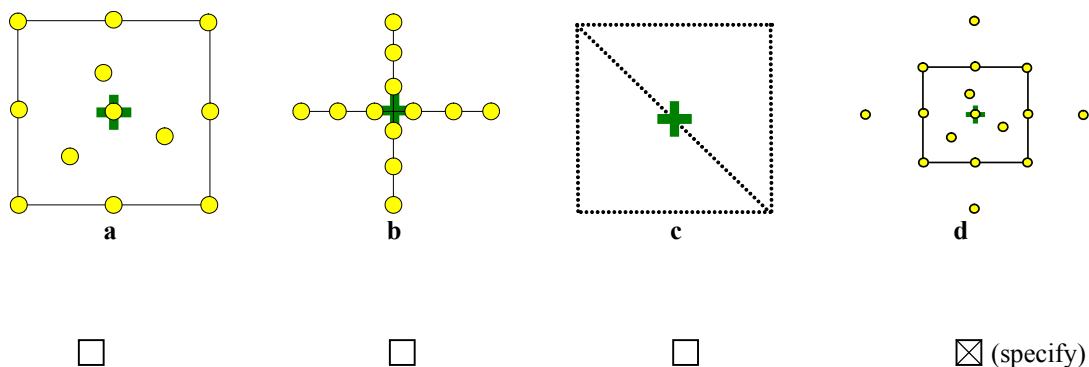
'd' strategy sampling contains 'a' strategy, we just add 4 extra picture points (out of 'a' square). Extra points are 10 m away from nearest neighbour point (like square points are 10 m away from centre point in horizontal or vertical direction) in horizontal or vertical direction. We decided to make 4 extra points because forest generally has bigger dimensions than agricultural field in term of plant size (Sylvain's idea).

Distribution of the Elementary sampling units

The crosses distribution with 4 extra points was used: 32 hemispherical photos are supposed to be taken over each ESU, 16 looking up (trees) and 16 looking down (understorey).

The high spatial resolution image

Satellite

Satellite used: SPOT2 HRVIR1
Level of processing: 2B SPOTVIEW Basic
Projection type: UTM 18 North/ WGS 84
Acquisition date: 19/08/2003

The image was provided by doing an ISIS command.
We order a 50 km circle centred on coordinates given on the following table.
The image was geo-referenced by SPOT image.

Georeferencing accuracy: 1 to 2 spot pixels.

3520*3809 pixels (20 by 20 m) image with 4 channels:

	Lat-Long WGS84 (Decimal Degree)		UTM / WGS84 Zone 18 North (m)	
	Lat.	Long.	Easting	Northing
Upper left corner	45.8131988	-75.75124759		
Lower right corner	75.2884935	-75.92835774		
Site centre				

Characteristics of the entire SPOT image

Preview of the SPOT image:
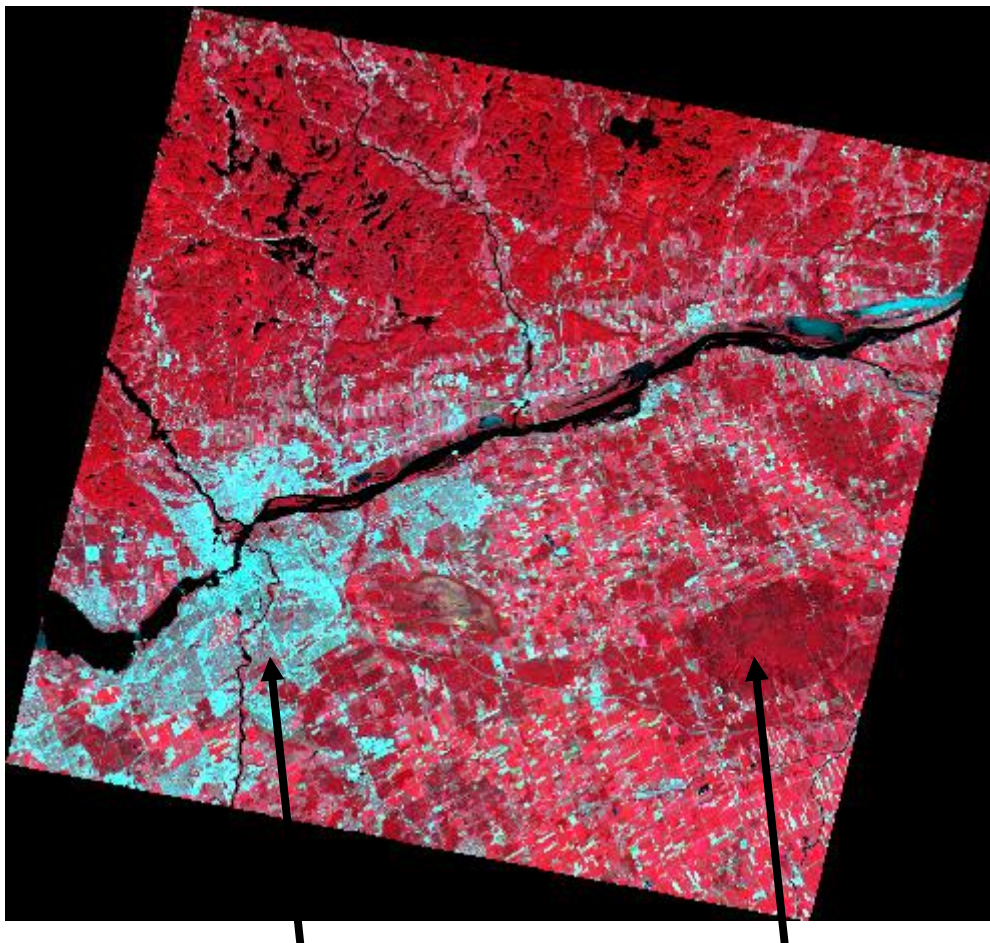
Ottawa, Ontario   **Larose Forest**

List of the ESUs

The GPSLarose2003.xls file contains the information for each ESU:

(ESU number 1 is done twice because for the first ESU we wanted to do an example)

| ESU#	Esting(m)	Northing(m)	Note
1	484381	5024785	Mixed deciduous forest (conifer-maple)
2	482715	5024617	Young trees, maple. Low underwood.
3	483974	5024817	Grass, low shrubland, young maple (and a lot of road)
4	482545	5024172	Young dense maple trees, with hole
5	483026	5024569	High density conifer, poor low underwood.
6	483806	5024616	High dense deciduous forest, low poor underwood.
7	484149	5024111	High density deciduous trees, low poor underwood.
8	482018	5024145	High density conifer, sometimes mixed with deciduous, low underwood, dead trunk, water.
9	481769	5023985	High density deciduous trees, low dense underwood, often water trace and dead trunk.
10	482295	5025144	High dense deciduous trees (maple and other), low dense under wood.
11	482334	5025632	Various height but not low dense deciduous trees, 1-2 m high dense under wood.
12	482242	5025465	High dense deciduous, 1m dense under wood with water sometimes.
13	482095	5026309	High dense mixed deciduous and conifer, low poor underwood.
14	482200	5025984	Wetland, grass and sometimes shrub growing on the water surface.
15	481895	5026191	Not very high and dense mixed deciduous, water on 1m dense under wood.
16	483110	5026239	Wetland, 4m deciduous trees mixed to dense shrub.
17	483355	5026454	High density conifer, pretty dense under wood 1-2m high, with maple sometimes.
18	483206	5026153	Broadleaf shrub 3m, wetland, grass sometimes.
19	483772	5025983	High density and low density deciduous trees, high density and low density 1-m underwood.
20	483660	5025880	Mixed conifer deciduous, dominant conifer, high density, low density underwood.
21	484004	5025203	Mixed conifer deciduous, on a wetland (so variable density), dense mixed under wood.
22	483806	5026345	Wetland in deciduous trees, pretty dense, underwood of very dense shrub.
23	481520	5024203	High density mixed spruce aspen, variable density of underwood.
24	484044	5024353	Wetland, shrub and high shrub (2-3m), high density.
25	483000	5025251	Wetland, high density 1m shrub, there's grass and dead wood too.
26	482740	5024911	High density conifer, path through it, low under wood, variable density.
27	482505	5025456	High with high density young aspen, dense 1-2m underwood with maple.
28	483300	5025492	Wetland, 2-3m shrub, grass, dead wood, good density.
29	483300	5024999	High density conifer, low to 1m not very dense underwood.
30	483104	5024406	Centered ESU on the Road, deciduous trees, not dense of course, water and grass.
31	482775	5024339	ESU centered on the road, on side high density conifer and the other deciduous.
32	484255	5026726	Dense mature conifer, low poor underwood.
33	483908	5023920	High density conifer, not very dense underwood (path trough it) with maple growing to 15m.
34	481606	5024822	High density deciduous, dense 1-1.5m underwood.

VALERI ESU's position on a 3 by 3 square for Larose 2003
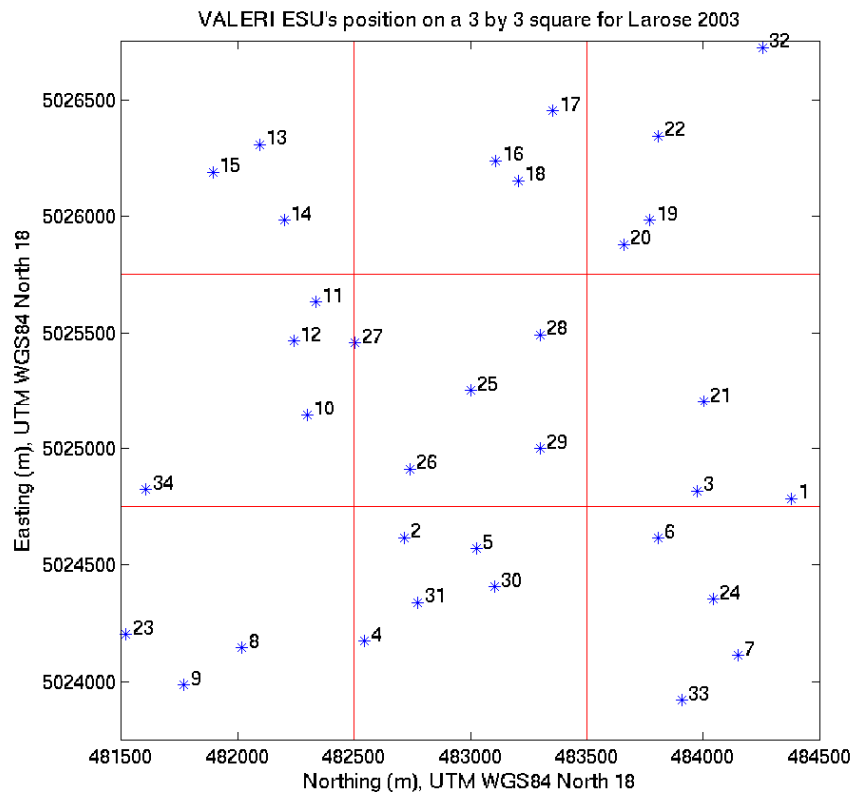
Acknowledgements

Thanks to Richard who managed to find ESU's in this so nice forest.
Thanks to Sylvain who took half of pictures and brought his forest sampling experience.
Thanks to Jujuan Li from CCRS for its participation.
Thanks again to Richard and Sylvain and their so animated talks about work.
Thanks to Forest State guards to let us do the job.

Photo gallery

The photos illustrating the campaign are to be stored in the directory "photo gallery" and the labels should be indicated in the table above.

For each ESU a panoramic photo was taken, the photo name is the ESU_*number*_panorama.

#	File name	Comments
1	ESU_X_panorama.jpg	ESU number X panoramic photo
2	Little_friend.jpg	Little animal on the road (Sylvain)
3	warning_english.jpg	Warning message for Larose wildlife (English)
4	warning_french.jpg	Warning message for Larose wildlife (French)
5	lunch_near_Larose2_030807.jpg	Lunch near Larose forest on third day, food wasn't good
6	what_to_wear2.jpg	What to wear to sample Larose (end of campaign)
7	all_samplers.jpg	Full members of Larose campaign (end of campaign)
8	all_samplers_from_canada.jpg	Canadian members of Larose campaign (beginning of campaign)
9	what_to_wear.jpg	End of campaign

Additional comments

ESU number 1 is done twice because for the first ESU we wanted to do an example.
Problems with two cameras (the two working with 4 batteries):
- One hemispheric camera seemed not to work very good at the end of the campaign (zoom locked, only working in Manual mode, and to switched power off user must take off batteries).
- One other hemispheric camera seemed not to work at the end of the campaign (user can't switch on power).

What to wear to do the sampling (ask CCRS they may have it for you):
- There were a lot of mosquitos (sampler must take a bug short, a thick pair of trousers).
- It could be a very wet site and it was in summer 2003 so sampler must take a pair of rain boots.

It is more convenient to rent a 4*4 car for the campaign. 4 big roads are going through the site but there are many dusty paths and because of the water a high car is nice. It's ok for walking because even if you have that kind of car, you will have to walk a lot.

Errors Made During the Campaign: how to ease treatment of hemispherical pictures (for example CAN-EYE Software)

1. Taking pictures down:
   Try to hide yourself as most as possible and your bag and other people and other instruments.

Wrong   **Good**
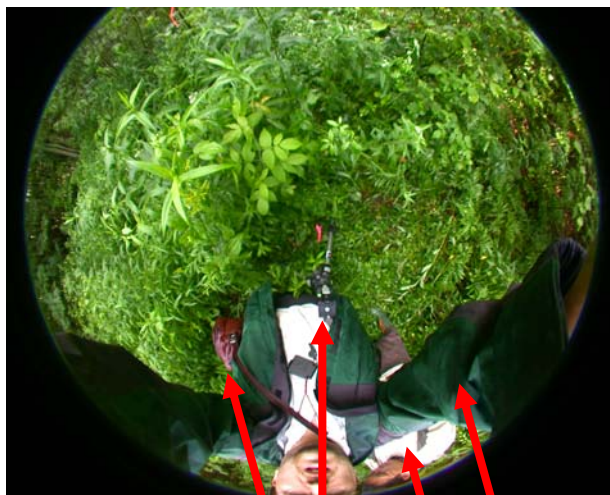
Bag

Hands

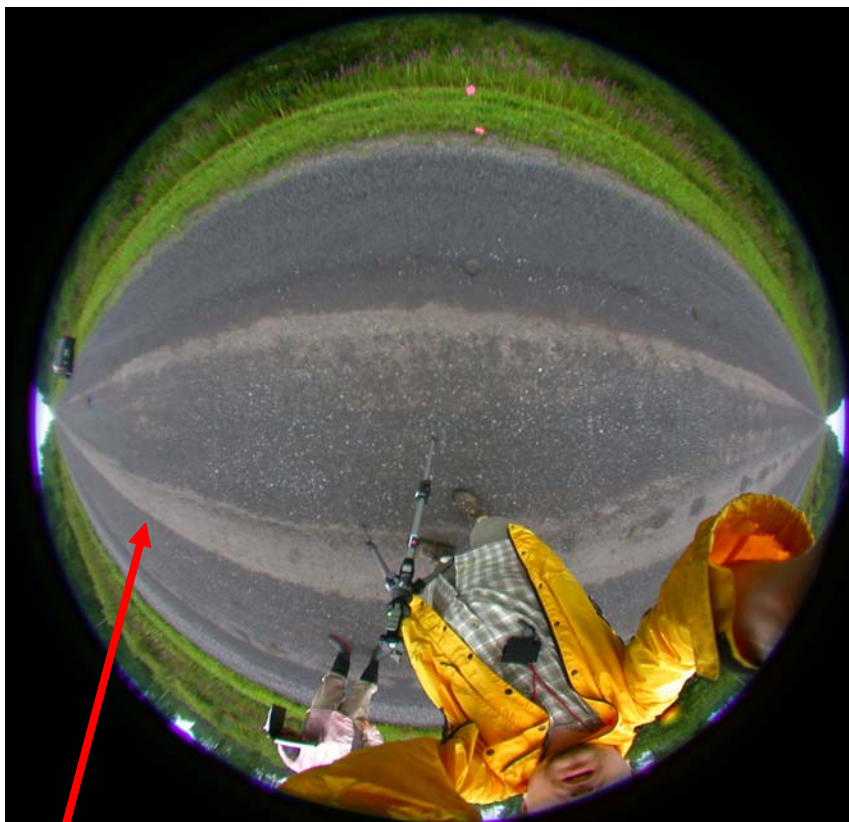**Other People**

Other instrument

Always take picture in the same direction: not a lost of info but a lost of time processing.

2 Different Positions for the Sun for one ESU

2. Not including paved roads in the picture: it's adding bad information.

Roads must be far from measurements

3. Be careful of the water under the lens: to be masked during the processing… takes time.

Residual Rain